A Computer Simulation Model for Proton Transport in Liquid Imidazole†

Hanning Chen,§ Tianying Yan,‡ and Gregory A. Voth*,§

Center for Biophysical Modeling and Simulation, Department of Chemistry, University of Utah, 315 South 1400 East, Room 2020, Salt Lake City, Utah 84112-0850, and Institute of New Energy Material Chemistry and Department of Material Chemistry, Institute of Scientific Computing, Nankai University, Tianjin 30071, China

Received: December 17, 2008; Revised Manuscript Received: February 1, 2009

A multistate empirical valence bond (MS-EVB) model is developed to simulate proton transport in liquid imidazole. This approach allows proton transfer to simultaneously occur on both reaction sites (donor and acceptor) of the imidazole molecule. The underlying imidazole and imidazolium models are described by the generalized Amber force field (GAFF). The imidazole MS-EVB model was parametrized to reproduce the ab initio proton shuttling potential energy surface (PES) of a protonated imidazole dimer in the gas phase. In bulk phase at 393 K, the MS-EVB simulation yields a proton diffusion coefficient of 0.20 $Å^2$/ps and a Grotthuss hopping rate of 1/36 ps^{-1}. Both results are in good agreement with experimental results. Despite the prevalence of a classical-like imidazolium structure with highly localized protonic charge, charge delocalization is not a negligible process in the simulations. Rather, it is shown to enhance the rate of proton diffusion by approximately 40% through Grotthuss shuttling. Analysis of the EVB states reveals that the imidazolium ion's first solvation shell by imidazole molecules is highly ordered through the formation of hydrogen bonds, while the second solvation shell is highly disordered. Together with the importance of charge delocalization, this result suggests that reorientation of imidazole rings in the second solvation shell is the rate-limiting step for proton transfer.

1. Introduction

The electrical conductivity of the imidazole crystal, discovered a number of years ago,[1] is generally attributed to proton transfer.[1−3] In addition to efforts to examine the role played by an imidazole moiety in proton-transfer reactions in biological systems,[4] there is a growing interest in using imidazole and its derivatives as the electrolyte in proton-exchange membrane (PEM) fuel cells at intermediate temperatures (120−200 °C).[5] An ideal electrolyte for this purpose would allow fast proton transport but inhibit electron conduction. The most widely used PEM, perfluorosulfonic polymer Nafion in the hydrated state, is strongly dependent on water for proton transport and thus limited by a relatively low operating temperature (less than 80 °C, so that the water does not evaporate).[6−8] Although it has long been demonstrated that the proton conductivity of liquid imidazole (its melting point is 90 °C[2]) can be as high as that of an aqueous solution of imidazole,[9] widespread interest in this compound has mainly come with the search for a replacement fuel cell electrolyte.[10]

Swollen polymer membranes with a mixture of ionic liquid and imidazole as the electrolyte have been tested.[11−15] Polymerizable ionic liquids have also been proposed as a new type of electrolyte.[16] Attempts have been made to develop a solid-state, proton-conducting polymer using immobilized, imidazole-based oligomers such as ethylene-oxide-tethered imidazole heterocycles (imi-*n*EO). In this scenario, the imidazole moieties are tethered to the polymer backbone via flexible spacers.[17,18] Recently, the use of heterocyclic compounds in the PEM electrolyte has also motivated Liu and co-workers to propose triazole as a proton-conducting medium.[19−21]

In the pioneering work of Kreuer et al.,[10] heterocyclic compounds such as imidazole, pyrazole, and benzimidazole were demonstrated to exhibit rather high proton conductivities. At a temperature roughly 30 °C higher than its melting point, liquid imidazole displays a level of proton diffusion comparable to that of water at ambient conditions. Moreover, the latter study demonstrated that the Grotthuss mechanism[22,23] (structural diffusion) plays an important role in proton transfer within liquid imidazole. The proton diffusion coefficient (D_θ) calculated from conductivity, according to the Nernst−Einstein relation, is distinctly higher than the self-diffusion coefficient (D_H) of hydrogen atoms measured by pulsed magnetic field gradient NMR spectroscopy. Had protons been conducted exclusively through the vehicular mechanism by imidazolium, which would yield a diffusion rate similar to that of the underlying imidazole molecules, the D_θ and D_H coefficients would be nearly equal. Instead, it was found that $D_\theta/D_H = 4.5$ in a dilute solution of sulfanilic acid in imidazole at 90 °C. The same ratio was measured to be approximately 2 at 120 °C.[10,24] Later, Watanabe et al. mixed bis(trifluoromethanesulfonyl)amide (HTFSI) with solid imidazole to obtain eutectics, which are liquid at room temperature.[12,25] Complete dissolution of HTFSI was observed in the imidazole-rich system, owing to the strong basicity of imidazole as identified by the ^1H NMR spectra, and proton transport was indicated between imidazolium cations and imidazole molecules in the presence of excess imidazole molecules. The Grotthuss mechanism and the vehicular mechanism therefore both contribute to proton conductivity in the above-mentioned systems.

Solid-state NMR spectroscopy has been used to probe the dynamics of proton transfer in an imidazole crystal,[26−28] imidazolium methylsulfonate,[28,29] and solid PEMs such as imi-

† Part of the "George C. Schatz Festschrift".

* To whom correspondence should be addressed. E-mail: voth@chem.utah.edu. Phone: (801) 581-7272. Fax: (801) 581-4353.

§ University of Utah.

‡ Nankai University.

10.1021/jp811156r CCC: $40.75 © 2009 American Chemical Society
Published on Web 03/10/2009

*n*EO with imidazole moieties linked to a linear polysiloxane backbone or a cyclic siloxane oligomer.[27,28,30] In such PEMs, proton transfer between imidazole moieties occurs principally through the Grotthuss mechanism. However, doubt has been cast on the existence of proton transfer in imidazole crystals because no reorientation of imidazole rings, widely considered the rate-limiting step in such systems, was detected on time scales up to several seconds in a ^{15}N 2D exchange NMR study.[26] High-resolution solid-state ^{1}H, ^{13}C, and ^{15}N NMR studies revealed that ordered and disordered domains coexist in crystalline imidazole and imi-*n*EO. It is the disordered regions that primarily contribute to proton conductivity.[27,28] In these systems, charge defects formed by proton doping interrupt the one-dimensional hydrogen-bonding network and induce rotational defects.[24,31,32] The resonance at 10 ppm in the ^{1}H NMR spectra was attributed to mobile hydrogen, but with much weaker dipolar interactions because of the broken hydrogen bonds.[27] Car−Parrinello molecular dynamics (CPMD) studies[31,32] carried out later by Iannuzzi and Parrinello showed that imidazole molecules are involved in the rotational defects that contribute to the 10 ppm resonance. Furthermore, the activation energy for ring reorientation was found to correlate well with that for proton mobility in a solid-state proton-conducting material,[28] where protons diffuse mainly via the Grotthuss mechanism.

In addition to the experimental and simulation efforts just discussed, a few additional computational studies have been performed to investigate proton transport in imidazole and its derivatives. An ab initio electronic structure calculation for a one-dimensional, infinite imidazole chain confirmed that conductivity in the imidazole crystal can be due to proton transport.[3] In another ab initio study, it was found that once an imidazole molecule approaches an ammonia molecule, proton transfer takes place with very little energy barrier, and translational motion was therefore the rate-limiting step.[33] A more detailed investigation of the potential energy function for an imidazole/imidazolium dimer revealed quite complicated interaction modes.[34] Specifically, the reaction barrier is very sensitive to the intermolecular nitrogen−nitrogen distance.[35] A more systematic investigation of proton transfer involving methyl imidazole as the conducting medium was recently performed, with a focus on explicitly designable PEMs for fuel cell applications.[36]

To study proton-transport dynamics in imidazole and its derivatives, CPMD simulations were performed on a pristine, protonated imidazole crystal[24,31,32] and an im-2EO oligomer.[31,32] The Grotthuss mechanism was observed in all of these CPMD simulations. The first CPMD simulation of an imidazole crystal[24] suggested that proton transfer is fast; therefore, reorientation of the rotational defect was taken to be the rate-limiting step. Moreover, proton hopping was identified as a local process without long-range or long-time coherent reorientations, similar to proton transfer in liquid water.[37−40] Iannuzzi and Parrinello[31,32] also performed a CPMD simulation with meta-dynamics (MTD)[41] and proposed that diffusion of the rotational defect, a process involving serial hydrogen bond forming and breaking, is the rate-limiting step for the proton transfer in both the imidazole crystal and im-2EO oligomer. That is, fast proton hopping is favored by a large separation between the protonic charge and the rotational defect.[31,32] Interestingly, this CPMD simulation also revealed that two structures could accommodate the excess proton, a Zundel-type structure where the proton is shared by two imidazole molecules (Im···H^+···Im), and an Eigen-type structure where the excess proton is highly localized on a imidazole molecule (Im···ImH^+···Im). The Eigen-type structure seems to be more stable as the temperature drops to 0 K.[32]

With a goal of overcoming the problem of "platinum poisoning" (due to the high binding energy of imidazole on a platinum surface),[42] Deng et al. proposed fluorinated imidazole and 2,4,5-trifluoroimidazole (ImF_3) as a novel anhydrous medium with much weaker binding to the platinum surface.[35] By estimating proton-hopping probabilities according to an ad hoc proton-hopping algorithm,[43] their study conducted stochastic MD simulations of a Nafion membrane using either imidazole or ImF_3 as the electrolyte.[35] That work indicated that the large size of fluorine atoms can significantly retard proton diffusion in ImF_3, implying a sensitivity of proton mobility to the distance between the hydrogen bond donor and acceptor. However, no appreciable correlation was observed between proton hopping and the reorientational dynamics of the imidazolium ring in either simulation.[35]

CPMD simulations are extremely demanding computationally and therefore limited to exploring small systems over short time scales, for example, tens of picoseconds for systems consisting of several imidazole crystal unit cells. It is therefore not surprising that the first CPMD simulation had too little integration time to observe reorientation of the imidazole rings.[24] In the later CPMD simulations employing the MTD methodology, real dynamical trajectories were not produced. (MTD employs a time-dependent potential energy surface to enhance phase space exploration, artificially encouraging the proton in this case to overcome the rather high energy barrier in a relatively short time.) Thus, although CPMD simulations have provided valuable information on the proton-transfer mechanism, their results must be considered speculative due to the very limited number of proton-transfer events studied. Furthermore, any dynamical model based on transition-state theory is fundamentally stochastic, making the interpretation of time-correlated properties a complicated proposition.

An efficient and reliable MD methodology that can provide long-time, deterministic trajectories is therefore highly desirable to further our understanding of proton conduction in liquid imidazole. To this end, the present paper describes a multistate empirical valence bond (MS-EVB) model.[37,38,44−46] The model takes into account both proton reaction centers (donor and acceptor) on the proton-conducting imidazole molecule. The structural, energetic, and dynamical properties of proton transport in liquid imidazole are then examined from MD simulations in the bulk phase with the MS-EVB model.

The sections of this paper are organized as follows. In section 2, the methodology and model are described in detail, while in section 3, results from the liquid-phase simulations are presented and discussed. This latter section focuses on proton transfer via the Grotthuss mechanism and its correlation with the solvation structure of the excess proton. Finally, section 4 summarizes what has been learned from this study and provides concluding remarks.

2. Methods

2.1. Parameterization of the Underlying Imidazole and Imidazolium Models. Because any MS-EVB model[37,38,44−46] is dependent on the underlying molecular models for the unprotonated and protonated entities, we first discuss the parametrization of imidazole and its protonated form, imidazolium. The general Amber force field (GAFF)[47,48] was chosen to describe intra- and intermolecular interactions for both species. GAFF has been proven to reliably automate force field

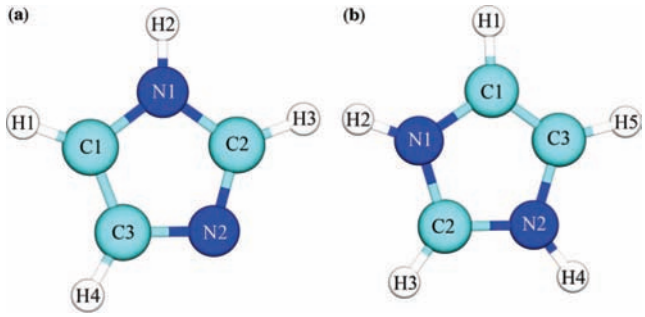

Figure 1. Atom names for the (a) imidazole and (b) imidazolium cation.

TABLE 1: Amber GAFF Atom Types, Partial Charges, and VDW Parameters for Imidazole (a) and Imidazolium (b)

atom name	GAFF atom type	q (e)	σ (Å)	ε (kcal/mol)
	(a) Imidazole			
C1	CD	−0.3353	3.399713	0.086
N1	NA	−0.2214	3.250040	0.170
C2	CD	0.2030	3.399713	0.086
N2	NC	−0.5348	3.250040	0.170
C3	CC	0.1469	3.399713	0.086
H1	H4	0.2137	2.510584	0.015
H2	HN	0.3110	1.069092	0.0157
H3	H5	0.1111	2.421493	0.015
H4	H4	0.1058	2.510584	0.015
atom name	GAFF atom type	q (e)	σ (Å)	ε (kcal/mol)
	(b) Imidazolium			
C1	C2	−0.1279	3.399713	0.086
N1	NA	−0.1469	3.250040	0.170
C2	C2	0.0650	3.399713	0.086
N2	NA	−0.1469	3.250040	0.170
C3	C2	−0.1279	3.399713	0.086
H1	H4	0.2513	2.510584	0.015
H2	HN	0.3710	1.069092	0.0157
H3	H5	0.2400	2.421493	0.015
H4	HN	0.3710	1.069092	0.0157
H5	H4	0.2513	2.510584	0.015

generation for a large number of organic molecules, including heterocycle-ring-based biological stereoisomers.[49] Nevertheless, other popular force fields such as OPLS-AA[12] and DREADING[50] are likely to offer a similar quality of molecular modeling. All of these approaches are also calibrated using the geometries and energies of gas-phase molecules optimized by ab initio electronic structure calculations.

Similar to other all-atom force fields, GAFF assigns a type to each atom according to its orbital hybridization and bonding connectivity. The individual names of atoms in the imidazole and imidazolium molecules are illustrated in Figure 1a and b, respectively. The partial atomic charges of both molecules, listed in Table 1, were determined by the Restrained Electrostatic Potential (RESP) method[51,52] using Hartree−Fock theory and the 6-31G* basis set. The GAFF types assigned to each atom are also shown in Table 1. The intramolecular bonded interactions, namely, bond stretching E_b, angular bending E_a, and dihedral twisting E_d, are uniquely determined by the GAFF types of the participating atoms. The functions employed by GAFF to reflect these three interactions can be written as follows

$$E_b = \sum_{N_b} \frac{1}{2} k_{b,ij}(r_{ij} - r_{ij,o})^2 \quad (1)$$

$$E_a = \sum_{N_a} \frac{1}{2} k_{a,ijk}(\theta_{ijk} - \theta_{ijk,o})^2 \quad (2)$$

$$E_d = \sum_{N_d} k_{d,ijkl}[1 + \cos(m_{ijkl}\phi_{ijkl} - \phi_{ijkl,o})] \quad (3)$$

where r_{ij}, θ_{ijk}, and ϕ_{ijkl} are the intramolecular bond length, valence angle, and dihedral angle, respectively. The symbols $k_{b,ij}$, $r_{ij,o}$, $k_{a,ijk}$, $\theta_{ijk,o}$, $k_{d,ijkl}$, m_{ijkl}, and $\phi_{ijkl,o}$ are predetermined empirical parameters, itemized in Table 2. As an exception to the usual GAFF approach, the Morse potential was used in this work rather than a harmonic potential to represent bond stretching between atoms of types NA and HN in imidazolium. This change is an effort to more properly describe the reactive characteristics of this chemical bond, particularly at long bond lengths. The Morse potential function is given by

$$E_{b,NA-HN} = k_{b,NA-HN}\{1 - \exp[-a_{b,NA-HN}(r_{NA-HN} - r_{NA-HN,o})]\}^2 \quad (4)$$

where the empirical parameters $k_{b,NA-HN}$, $a_{b,NA-HN}$, and $r_{NA-HN,o}$ are 145.637 kcal/mol, 1.011 Å^{-1}, and 1.04823 Å, respectively. The parameter r_{NA-HN} is the length of the imidazolium NA−HN bond.

Nonbonded interactions E_{nb} were treated as a standard combination of the electrostatic and van der Waals (VDW) forces

$$E_{nb} = \sum_{N_{nb}} \left\{ \frac{q_i q_j}{r_{ij}} + 4\varepsilon_{ij}\left[\left(\frac{\sigma_{ij}}{r_{ij}}\right)^{12} - \left(\frac{\sigma_{ij}}{r_{ij}}\right)^{6}\right]\right\} \quad (5)$$

where r_{ij} is the distance between two atoms and the q's are atomic partial charges. The interatomic VDW parameters, ε_{ij} and σ_{ij}, are determined by the Lorentz−Berthelot mixing rule

$$\varepsilon_{ij} = \sqrt{\varepsilon_i \varepsilon_j} \quad (6)$$

$$\sigma_{ij} = \frac{1}{2}(\sigma_i + \sigma_j) \quad (7)$$

The values of the VDW parameters are listed in Table 1. Note that the intramolecular 1−4 electrostatic and VDW interactions are scaled by factors of 0.833 and 0.500, respectively, following current practice in the AMBER94 force field[9] and its more recent variants.

2.2. The MS-EVB Framework for an Excess Proton in Liquid Imidazole. Fundamentally, a solvated proton cannot be distinguished as being associated with a certain imidazole molecule to form protonated imidazolium. The case of an excess proton in liquid imidazole represents a system in which an imidazolium cation cannot be defined as in the classical imidazolium model described in section 2.1. The best way to describe an imidazolium in liquid imidazole is to partition the system into multiple diabatic EVB states so that the adiabatic ground state of the system can be described as a linear combination of these diabatic EVB states, with each of the latter having different probability amplitudes according to the variational principle.[44]

TABLE 2: Intramolecular interaction parameters for imidazole and imidazolium

bond stretching parameters			angular bending parameters			dihedral twisting parameters			
bond	$k_{b,ik}$(kcal/mol//Å^2)	$r_{ij,o}$(Å)	angle	$k_{a,ijk}$(kcal/mol/rad^2)	$\theta_{ijk,o}$(deg)	dihedral(*improper type)	$k_{d,ijkl}$(kcal/mol)	m_{ijkl}	$\phi_{ijkl,o}$(deg)
CD−H4	700.02	1.083	CC−CD−H4	94.40	129.11	CC−NC−CD−H5	4.75	2.0	180.0
CD−NA	877.60	1.371	NC−CC−H4	100.0	120.03	CC−CD−NA−HN	1.70	2.0	180.0
CD−CC	1008.0	1.371	CD−CC−H4	94.40	129.11	CD−NC−CC−H4	4.75	2.0	180.0
CD−H5	712.00	1.079	NC−CD−H5	100.2	125.38	NA−CD−CC−H4	4.00	2.0	180.0
CD−NC	989.20	1.335	CD−NA−HN	94.40	124.66	H4−CC−CD−H4	4.00	2.0	180.0
NC−CC	863.20	1.376	NA−CD−H5	99.60	122.10	NC−CC−CD−H4	4.00	2.0	180.0
CC−H4	700.20	1.083	NA−CD−H4	100.4	119.66	NC−CD−NA−NA	1.70	2.0	180.0
NA−HN	813.20	1.011	CC−NC−CD	141.0	107.47	CD−NA−CD−H4	1.70	2.0	180.0
C2−H4	697.20	1.084	NA−CD−CC	145.8	109.42	H5−CD−NA−CD	1.70	2.0	180.0
C2−NA	822.20	1.391	CD−CC−NC	142.0	114.98	H5−CD−NA−HN	1.70	2.0	180.0
C2−C2	1179.4	1.324	NC−CD−NA	149.6	112.02	H4−CD−NA−HN	1.70	2.0	180.0
C2−H5	715.00	1.078	CD−NA−CD	137.2	109.90	CD−CD−NA−HN*	1.10	2.0	180.0
			C2−NA−HN	95.20	119.28	CC−NC−CD−NA	4.75	2.0	180.0
			C2−C2−H4	98.60	124.68	CC−CD−NA−CD	1.70	2.0	180.0
			NA−C2−H4	100.8	116.25	NC−CC−CD−NA	4.00	2.0	180.0
			NA−C2−H5	96.60	126.39	NC−CD−NA−CD	1.70	2.0	180.0
			C2−NA−C2	135.6	110.37	CD−CD−NC−CD	4.75	2.0	180.0
			C2−C2−NA	139.6	121.38	C2−NA−C2−H5	0.63	2.0	180.0
			NA−C2−NA	147.4	109.33	C2−C2−NA-HN	0.63	2.0	180.0
						H4−C2−NA−C2	0.63	2.0	180.0
						H4−C2−NA−NA	0.63	2.0	180.0
						H4−C2−C2−NA	6.65	2.0	180.0
						H4−C2−C2−H4	6.65	2.0	180.0
						NA−C2−NA−HN	0.63	2.0	180.0
						H5−C2−NA−HN	0.63	2.0	180.0
						C2−C2−NA−HN*	1.10	2.0	180.0
						C2−NA−C2−NA	0.63	2.0	180.0
						C2−C2−NA−C2	0.632	2.0	180.0
						NA−C2−C2−NA	6.65	2.0	180.0

With the above partitioning of the EVB states in mind, the MS-EVB methodology is capable of simulating proton transfer as a multipathway reaction. It can model the formation and breakage of chemical and hydrogen bonds in protonated liquid imidazole according to its Grotthuss mechanism.[10,11] Like water, imidazole has an extensive network of hydrogen bonds. This means that the proton donor and proton acceptor need only minimal displacements to cause a transfer to occur, facilitating rapid proton transport. Moreover, the formation of a stable protonated imidazolium core is to be expected given the strong affinity of excess protons to electrons and their consequential tendency to form chemical bonds with any nearby proton acceptor. In this case, a non-hydrogen-bearing nitrogen atom in imidazole accepts the excess proton, resulting in the formation of imidazolium. In other words, proton translocation in an imidazole medium is equivalent, at least in part, to a change in the imidazolium cation's identity. Proton transfer is also responsible for fluctuations in the imidazolium's solvation structure, as depicted in Figure 2 for a linear protonated imidazole trimer. As Figure 2 shows, each of the two imidazole nitrogen atoms can either donate a proton (the hydrogen-bearing nitrogen atom) or accept a proton (the non-hydrogen-bearing nitrogen atom). An imidazole molecule thus has two hydrogen-bonding reaction centers, whereas a water molecule just has one. Such structures with multiple reaction centers are widely present in heterocyclic compounds. Although the two reaction centers are believed to allow for intramolecular protonic charge transfer through tautomerization, typically with the aid of solvents,[53] the present study focuses exclusively on the Grotthuss shuttling mechanism for two reasons, (1) the energetic instability of ionized imidazole is prohibitively high, and (2) the absence of other molecular components in the imidazole system that can aid the tautomerization. These points will be investigated in more detail later.

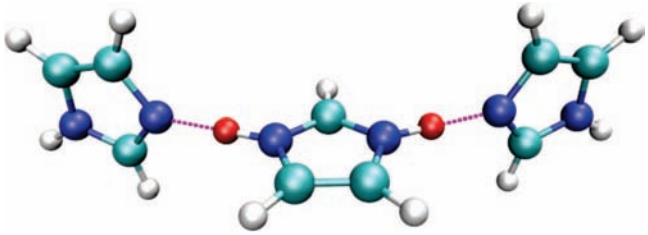

Figure 2. The structure of a linear, protonated imidazole trimer. The two transferring protons are shown in red. The hydrogen bonds formed between transferring protons and non-hydrogen-bearing nitrogen atoms are illustrated as purple dashed lines.

Although every possible hydrogen-bonding topology can be regarded as a so-called EVB state, within the framework of the MS-EVB model, only those EVB states that have non-negligible contributions to the ground-state energy of the system for a given configuration of the nuclei are counted for reasons of practicality. The most significant EVB states in the model imidazole systems were found according to the following state-searching algorithm:

(1) At every time step of a MS-EVB simulation, the pivot state refers to the imidazolium cation which had the largest EVB amplitude in the previous time step. For the first step, the imidazole molecule with the shortest distance between its non-hydrogen-bearing nitrogen atom and the excess proton is chosen as the pivot state and becomes imidazolium after accepting the excess proton.

(2) By regarding the pivot imidazolium as a reactant state for hydrogen bonding, any imidazole molecule can be considered a potential product state if the shortest distance between its non-hydrogen-bearing nitrogen atom and either of the two transferring protons of the pivot imidazolium is less than 2.5 Å, which represents the first minimum in R_{H^*-N}, as shown in Figure 7b below. The first solvation shell thus consists of two

imidazole molecules, either of which could constitute a new EVB state by accepting the closer proton and breaking the chemical bond between that atom and its donor.

(3) Each of the product EVB states formed in step 2 are treated as a reactant EVB state in turn. By repeatedly following the procedure described in step 2, the EVB states of the second solvation shell of the pivot imidazolium can be composed.

Although steps 2 and 3 can be iterated to include as many solvation shells as will fit within the simulation volume, two solvation shells were found sufficient for the imidazole systems studied in this work. The quality of the simulation can be determined by examining the conservation of total system energy in the constant NVE ensemble. This point will be discussed later in section 3.

In the MS-EVB approach, the solvation structure of the excess proton is conceptualized as a linear combination of those EVB basis states identified by the algorithm just described above, that is

$$|\Psi\rangle = \sum_{i}^{N} c_i(\mathbf{x})|i\rangle \tag{8}$$

In eq 8, $|\Psi\rangle$ is the adiabatic MS-EVB state as a function of all coordinates of the system $\mathbf{x}$, while the $|i\rangle$'s are the diabatic EVB basis states. An EVB Hamiltonian matrix, $\mathbf{H}$, is constructed with the elements $h_{nm}(\mathbf{x})$. In practice, these elements are represented by empirical force fields as described in section 2.1, as well as the off-diagonal elements which allow proton shuffling between imidazole molecules. The ground-state energy $E_0(\mathbf{x})$ of the protonated complex can be conveniently determined by solving the matrix eigenvalue equation according to the variational principle

$$\mathbf{c}^T\mathbf{H}\mathbf{c} = E_0(\mathbf{x}) \tag{9}$$

where $\mathbf{c}$ is a ground-state eigenvector whose elements are the coefficients $c_i(\mathbf{x})$ of eq 8. The system can be propagated using the force $\mathbf{F}_j(\mathbf{x})$ exerted on atom j at position $\mathbf{x}_j$, which can be calculated by the Hellmann−Feynman theorem as

$$\mathbf{F}_j(\mathbf{x}) = -\langle\Psi_0|\vec{\nabla}_j H|\Psi_0\rangle = -\sum_{m,n} c_m^*(\mathbf{x})c_n(\mathbf{x})\vec{\nabla}_j h_{mn}(\mathbf{x}) \tag{10}$$

The diagonal elements $h_{nn}(\mathbf{x})$ of the EVB Hamiltonian $\mathbf{H}$ represent the diabatic energies of the EVB basis states. For the protonated imidazole liquid system, the elements $h_{nn}(\mathbf{x})$ are given by the following expression

$$h_{nn}(\mathbf{x}) = V_{\text{imi}^+}^{\text{intra}} + \sum_{k}^{N_{\text{imi}}} V_{\text{imi}}^{\text{intra},k} + \sum_{k}^{N_{\text{imi}}} V_{\text{imi}^+,\text{imi}}^{\text{inter},k} + \sum_{k<k'}^{N_{\text{imi}}} V_{\text{imi}}^{\text{inter},kk'} \tag{11}$$

From left to right, the four terms are the intramolecular potential of the imidazolium cation, the intramolecular potential of the imidazole molecules, the intermolecular interaction between the imidazolium cation and the imidazole molecules, and the intermolecular interaction between the imidazole molecules. All four can be calculated from the GAFF force field, which was discussed in the previous section.

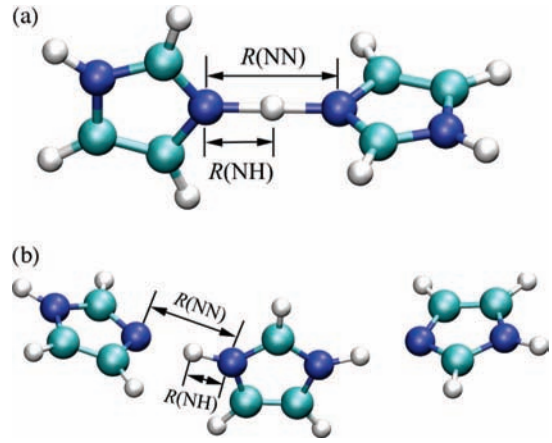

Figure 3. Gas-phase protonated imidazole dimer (a) and trimer (b).

As a reactive force field, the MS-EVB method can describe chemical processes (those involving chemical bond breaking and formation) by coupling the reactant state to the product state. In the present model, a pair of EVB states is considered coupled if their respective imidazolium cations share a common transferring proton. The off-diagonal elements $h_{nm}(\mathbf{x})$ of the EVB Hamiltonian $\mathbf{H}$ represent such chemical couplings and are defined by

$$h_{nm}(\mathbf{x}) = V_{\text{const}} \cdot A(R_{NN}, q_{NN}) \tag{12}$$

Here, V_{const} is an empirical coupling constant, and $A(R_{NN},q_{NN})$ is a damping function dependent on the geometry of the coupling adduct ImH^+-Im

$$A(R_{NN}, q_{NN}) = \exp(-\gamma q_{NN}^2)\{1 + P\exp[-k(R_{NN} - D_{NN})^2]\} \times \left\{\frac{1}{2}[1 - \tanh(\beta(R_{NN} - R_{NN}^0))] + P'\exp(-\alpha(R_{NN} - r_{NN}^0))\right\} \tag{13}$$

The quantity R_{NN} is the distance between the two adduct nitrogen atoms sharing the transferring proton, and the asymmetric stretch coordinate q_{NN} is the length of the vector connecting the point halfway between the adduct nitrogen atoms to the transferring proton. The complete set of empirical parameters for the MS-EVB model thus consists of γ, P, k, D_{NN}, β, R_{NN}^0, P', α, and r_{NN}^0, in addition to V_{const} in eq 12. The optimal determination of their values will be presented in the next section.

2.3. Parameterization of the Imidazole MS-EVB Model. Following the parametrization protocol of the MS-EVB3 model[46] for aqueous solutions, the imidazole MS-EVB model was based in part on a benchmark system, the ab initio potential energy surface (PES) of a protonated gas-phase imidazole dimer (illustrated in Figure 3). A previous study[13] has demonstrated that the proton-transfer energy profile between two imidazole molecules is principally dependent on two distances, R_{NN} between the proton donor and the proton acceptor and R_{NH} between the proton donor and the transferring proton (Figure 3). A two-dimensional, relaxed PES scan was performed along those two coordinates at the level of B3LYP/6-311G** DFT using the Gaussian 03 quantum chemistry software.[54] The PES of proton transfer so obtained is exhibited in Figure 4. The coordinate R_{NN} was varied from 2.64 to 2.94 Å, and R_{NH} was

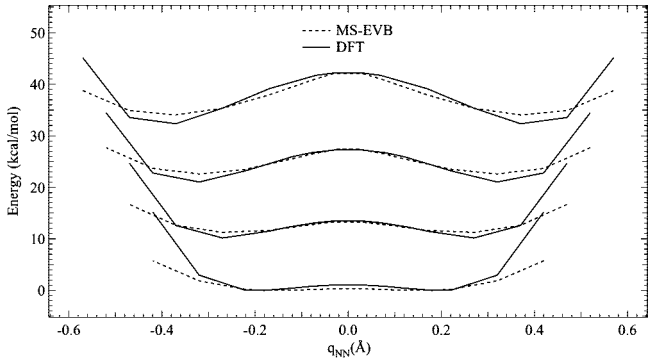

Figure 4. The potential energy surface (PES) of a protonated imidazole dimer. The *x*-axis (q_{NN}) is the asymmetric stretching coordinate described in eq 13. Cross sections of the PES are plotted for the following values of R_{NN} (see Figure 3): 2.64, 2.74, 2.84, and 2.94 Å. For visual clarity, the latter three curves are offset by 10, 20, and 30 kcal/mol, respectively, from their actual energy values. The solid curves (DFT) were calculated with the B3LYP/6-311G** level of theory. The dashed curves (MS-EVB) result from the optimal parameter choice in the present model.

TABLE 3: Parameters of the Imidazole MS-EVB Model

V_{const}	−13.63367	kcal/mol	γ	0.32349	Å^{-2}
P	0.19391		k	2.79839	Å^{-2}
D_{NN}	2.98451	Å	β	1.47107	Å^{-1}
R^0_{NN}	2.73998	Å	P'	1.19798	
α	6.61940	Å^{-1}	r^0_{NN}	1.81092	Å

varied from 0.9 to 1.5 Å, both with a step of 0.1 Å, for a total of 28 reference points.

All 10 MS-EVB parameters were included in the training set during the parametrization procedure, which minimized the root-mean-square deviation between the PES calculated from trial values of the parameters and the ab initio PES. The electronic polarization effect, though not explicitly included in the current model, was implicitly incorporated to a certain degree in the parameter fitting. The SIMPLEX algorithm[55] was employed to solve this nonlinear optimization problem. Ten weakly correlated and reasonably guessed initial parameter sets were fed into the SIMPLEX algorithm[55] to ensure the ergodic sampling of the parameter space. The resulting optimized parameter sets were further scrutinized by running MS-EVB simulations of a box of 216 imidazole molecules in the bulk phase; the set resulting in the highest-quality PES and most consistent experimental bulk properties was ultimately selected. The 10 parameters of this set are listed in Table 3, and the empirical PES obtained with those parameters is shown in Figure 4.

2.4. Computational Details. Unless otherwise specified, all of the MS-EVB simulations were carried out for a system composed of 216 imidazole molecules and 1 excess proton. The system was contained within a cubic volume of length 28.72 Å, providing a mass density of 1.03 g/cm^3. This value is consistent with the experimentally determined density of 1.0303 g/cm^3 observed at a temperature of 384 K.[56] Thermostatic properties such as the radial distribution function (RDF) were calculated in a constant NVT ensemble using the Nosé−Hoover thermostat,[57] which had a relaxation time of 0.2 ps, to maintain the system temperature at 393 K. At such temperatures, nuclear quantum effects are not likely to be important; therefore, the simulations were performed using classical mechanics. Dynamical properties such as the self-diffusion coefficient, on the other hand, were calculated from simulations performed in the constant NVE ensemble. For both kinds of calculations, a total of 40 ns was simulated, consisting of four independent 10 ns long simulations with distinct configurations of the initial system nuclei and momenta. Although the mean temperature of each NVE trajectory was, on average, ∼4 K off the target temperature at which the system had been equilibrated, no persistent heating or cooling was observed during these simulations. Three-dimensional periodic boundary conditions were applied in all simulations, and the system was propagated with a time step of 1 fs using the leapfrog algorithm to integrate Newton's equation of motion. Long-range electrostatics were treated by Ewald lattice summation[58] with a tolerance cutoff of 10^{-6}. A spherical truncation method with a cutoff radius of 9.0 Å was applied to the VDW interactions. The DL_EVB software, derived from the DL_POLY MD package (version 2.13),[59] was employed to perform the MS-EVB simulations. All of the analysis programs were developed in house.

TABLE 4: Geometrical Properties of the Optimized Protonated Imidazole Dimer and Trimer

cluster	property		MS-EVB	DFT/6-311G**
dimer	R(NN)	(Å)	2.55	2.57
	R(NH)	(Å)	1.28	1.29
	D^a	(deg)	97.82	92.37
trimer	R(NN)	(Å)	2.69	2.74
	R(NH)	(Å)	1.09	1.07
	D^b	(deg)	96.20	91.42
	D'^c	(deg)	156.19	150.81

[a] The dihedral angle between the planes of the two imidazole rings in the protonated dimer. [b] The dihedral angle between the planes of two proximate imidazole rings in the protonated trimer. [c] The dihedral angle between the planes of the two outer imidazole rings in the protonated trimer.

3. Results and Discussion

3.1. PES for Proton Transfer between Two Imidazole Molecules. The strongly hydrogen-bonded imidazolium−imidazole complex is the intermediate state of the proton transition; therefore, its PES is essential for governing the thermostatic and dynamical properties (reaction rate, solvation structure of imidazolium, etc.) of an excess proton solvated in imidazole. As shown in Figure 4, the present MS-EVB model reproduces well the ab initio PES for various proton donor−acceptor distances R_{NN}. The proton-transfer energy barriers for R_{NN} = 2.64, 2.74, 2.84, and 2.94 Å are approximately 1.1, 3.3, 6.3, and 9.9 kcal/mol respectively. Thus, even at a relatively high (e.g., fuel cell operation) temperature of ∼400 K, proton transfer between two imidazole rings is nearly prohibited when R_{NN} is greater than 2.74 Å. In contrast, when R_{NN} is as short as 2.64 Å, the energy barrier of ∼1.1 kcal/mol can easily be surmounted by thermal fluctuations. It can be inferred from this that proton-hopping events are likely to occur in the liquid.

3.2. Optimized Structures of the Protonated Imidazole Dimer and Trimer. To further assess the quality of the MS-EVB parametrization, the structure of a protonated imidazole dimer optimized using the MS-EVB model was compared to that obtained from the ab initio calculations. Because the imidazolium is typically solvated by its two proximate imidazole molecules in the condensed phase, forming two N−H−N type hydrogen bonds as illustrated in Figure 2, the optimized geometries of the protonated imidazole trimer were also examined. The key geometrical properties of the optimized dimer and trimer (shown in Figure 3) are summarized in Table 4, which indicates good agreement between the results of the MS-EVB model and the ab initio calculations.

3.3. Charge Defect Delocalization of the Excess Proton. As an indication of their proton-sharing propensity,[44−46] the extent of excess protonic charge defect delocalization among

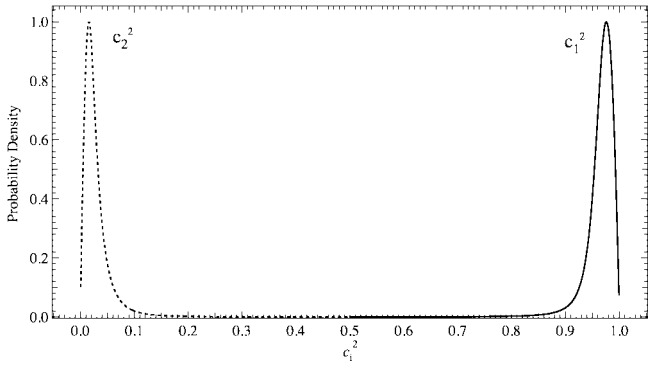

Figure 5. The probability distributions of the MS-EVB states with the largest (c_1^2) and the second-largest (c_2^2) amplitudes.

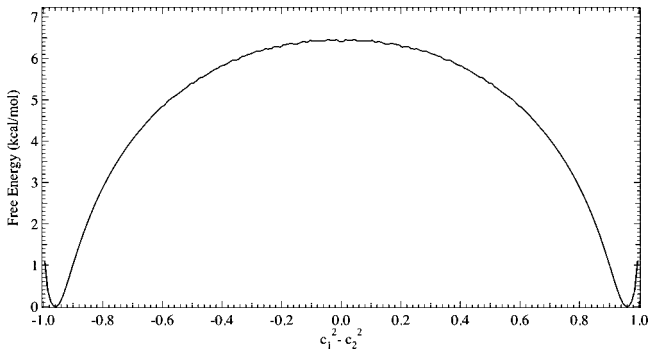

Figure 6. The free-energy profile for proton transfer along the order parameter defined as $c_1^2 - c_2^2$, the difference between the largest and second-largest EVB amplitudes.

imidazole molecules can be characterized by the probability distribution profiles of the two largest EVB amplitudes, c_1^2 and c_2^2 (Figure 5). In distinct contrast with water, where the states corresponding to c_1^2 and c_2^2 are broadly distributed and their peaks are only separated by ~0.45 along the coordinate axis of c_i^2,[46] in imidazole, the two profiles are rather sharp and separated. The peaks of the c_1^2 and c_2^2 states are located at 0.97 and 0.03, respectively. The excess proton charge is therefore localized mainly on a given imidazolium cation rather than among multiple solvating imidazole molecules, quite different from the behavior in water. The significant abatement of protonic charge delocalization in imidazole compared to water can be ascribed to two factors, the N—H bond is weaker than the O—H bond due to the diminished electronegativity of nitrogen compared to that of oxygen and the relatively long distance between the proton donor and proton acceptor in imidazole (see section 3.5 for details). The latter arises from steric hindrance by the aromatic ring structure. The prevalence of imidazolium with a nearly full positive charge was further confirmed by statistical analysis; during 98.2% of the MS-EVB simulation, the pivot imidazolium possessed 90% or more of the excess protonic charge. Nevertheless, Grotthuss-type proton hopping is still important for imidazole, as will be discussed in section 3.6, in particular, when the dynamical diffusive properties of the excess proton are considered. This process is not well described by a classical model of a fully charged imidazolium cation.

3.4. Proton-Transfer Process in Liquid Imidazole. A simplified "order parameter" can be defined for the proton-transfer process of an excess proton between two imidazole molecules as $c_1^2 - c_2^2$, that is, the difference between the largest and second-largest EVB amplitudes. The proton-transfer free-energy profile in the bulk phase can then be calculated using the probability distribution along that order parameter (Figure 6). As expected, given the fact that the excess protonic charge is highly localized around a given imidazolium, the free-energy profile exhibits a minimum at $c_1^2 - c_2^2 = 0.97$. This state corresponds to a nearly classical imidazolium cation. The peak of the free-energy profile is ~6.5 kcal/mol higher than the minimum free energy and is located at $c_1^2 - c_2^2 = 0$. This latter configuration represents a protonated imidazole dimer, where the two molecules equally share a transferring proton.

The height of the free-energy barrier along the order parameter defined above does not correlate well with the

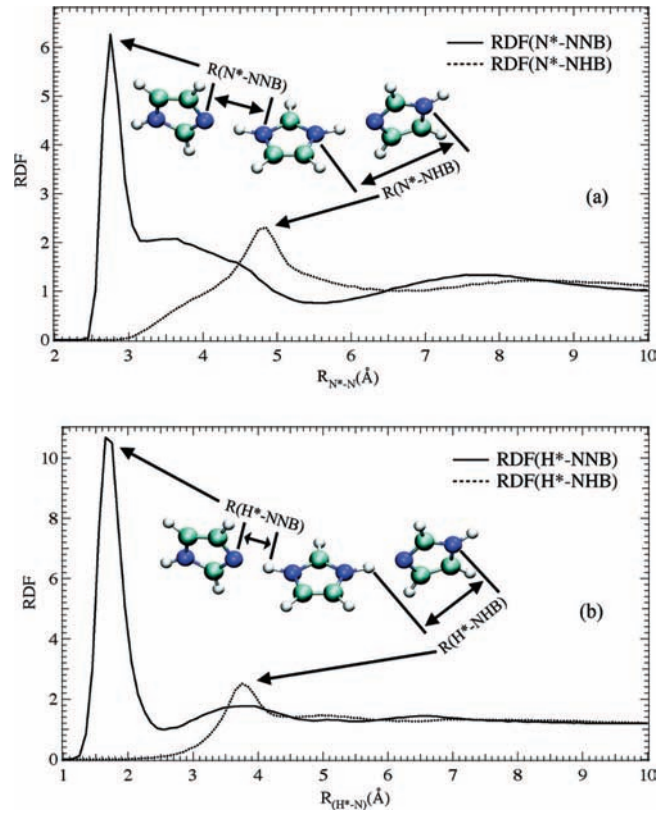

Figure 7. (a) Intermolecular radial distribution functions of non-hydrogen-bearing nitrogen atoms (NNB) and hydrogen-bearing nitrogen atoms (NHB) in imidazole around the imidazolium nitrogen atoms (N*). (b) Intermolecular radial distribution functions of NNB and NHB around the pivot imidazolium hydrogen atoms (H*).

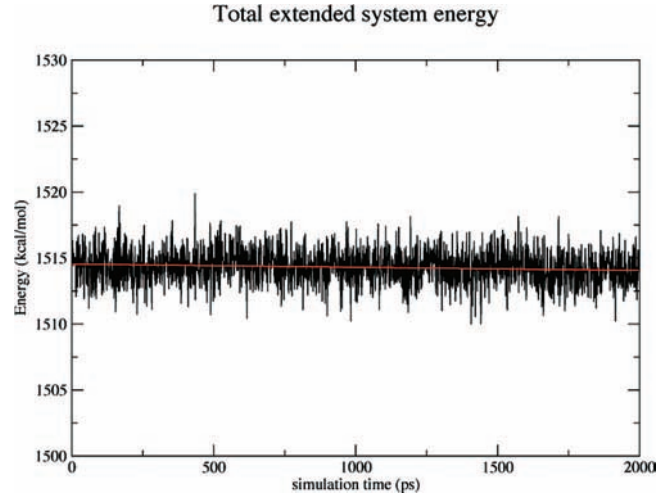

Figure 8. Total system energy conservation of a typical MS-EVB trajectory in the constant NVE ensemble, with a target temperature of 393 K.

calculated activation energy for the excess proton diffusion (see section 3.6 below). This suggests that a different reaction coordinate is operational for the proton-transport process. Given the relatively slow rate of intermolecular proton transfer in imidazole, the proton-hopping process can also be investigated by NMR spectroscopy,[47] the results of which suggest a similar conclusion. Since proton translocation in condensed phases usually involves a series of collective hydrogen bonding rearrangements,[60] for example, through multiple ring reorientations in imidazole,[1,24] a complete description of the reaction coordinate for proton hopping in liquid imidazole is clearly more complicated than the simple order parameter defined above.

3.5. Radial Distribution Functions. The solvation structure of the excess proton in imidazole can be quantitatively described by the radial distribution function (RDF) of imidazole molecules around the imidazolium. Because the two transferring protons of imidazolium are chemically identical, they were treated equivalently here and denoted as H*. A similar treatment was applied to its nitrogen atoms, denoted N*. In contrast, the two nitrogen atoms of imidazole are chemically distinguishable; one of them (denoted NHB) bears a transferring proton and thus can serve as a proton donor while the other (denoted as NNB) does not and can serve as a proton acceptor. Identification of the proton donor and acceptor in imidazole is clearly necessary because the solvation structure of imidazolium will reflect the hydrogen-bonding pattern as discussed below.

The RDFs of NNBs and NHBs around the pivot imidazolium nitrogen atoms, N*, are shown in Figure 7a. The first NNB solvation shell of N* is the sharp peak at ~2.8 Å, with a height of ~6.2. This peak decays smoothly from ~3.1 Å outward, reaching the first minimum at ~5.4 Å. In contrast, the second peak of RDF_{N^*-NNB} at ~7.8 Å is quite shallow and barely visible, indicating that the second imidazole solvation shell of the imidazolium is highly disordered. The broad first peak of RDF_{N^*-NHB}, centered at ~4.8 Å, suggests that the imidazole molecule in the first solvation shell is still relatively flexible; the ring can bend toward or away from the imidazolium to some degree, despite its anchored proton acceptor (NNB). This characterization of the two first peaks is confirmed by their separation of ~2.0 Å, which is very close to the intramolecular distance of 2.1 Å between the two nitrogen atoms.

The RDFs of NNBs and NHBs, relative to the imidazolium's transferring proton, H*, are displayed in Figure 7b. The acute first peak of RDF_{H^*-NNB}, located at ~1.7 Å with a height of ~10.9, clearly indicates the formation of a hydrogen bond between the imidazolium and imidazole in its first solvation shell. This relatively long hydrogen bond is the primary reason for the strong localization of protonic charge in imidazole. Similar to RDF_{N^*-NHB}, the first peak of RDF_{H^*-NHB} (centered at ~3.7 Å) is broadly distributed. Again, this feature can be ascribed to the moderate inter-ring pliability of the imidazolium−imidazole complex.

The imidazolium is typically fully charged and tends to have a strong association with the two imidazole molecules in its first solvation shell due to the significantly structured hydrogen bonds. In contrast, the correlation between the first solvation shell and second solvation shell imidazole molecules is rather weak. These molecules have minimal imidazolium characteristics because the excess protonic charge is strongly localized on the central imidazolium. The contrast between the highly ordered first solvation shell and the disordered second solvation shell suggests that the Grotthuss-type proton-hopping rate may be related to the likelihood of forming hydrogen bonds between the first and second solvation shells. Any identity change of the imidazolium has to be immediately stabilized by rebuilding the first solvation shell. In other words, reorientation of an imidazole molecule in the second solvation shell is likely to be the rate-limiting step of the proton-transfer reaction, as suggested from a previous CMPD study.[24]

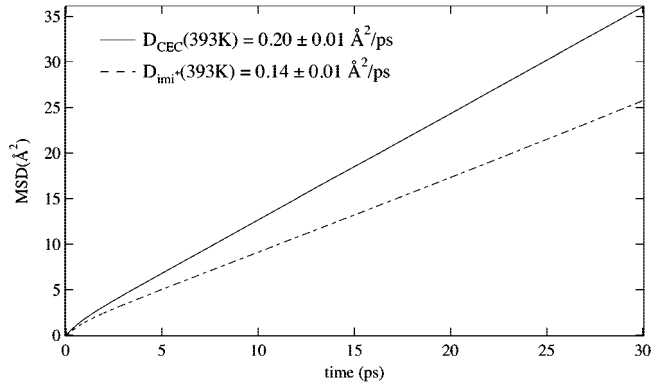

Figure 9. Mean-square displacements of center of excess charge (CEC) and classical imidazolium (Imi^+ with Grotthuss shuttling disabled in the MS-EVB algorithm) at 393 K as a function of time.

3.6. Proton Self-Diffusion Coefficient and Activation Energy. Because all of the dynamical properties were calculated from trajectories performed in a constant NVE ensemble, it was first necessary to monitor the conservation of energy to ensure a sampling of the proper phase space. The total system energy, depicted in Figure 8, exhibits an almost negligible drift rate of 0.3 kcal mol^{-1} ns^{-1} as the simulation progresses. Moreover, this excellent energy conservation validates the decision to use only two imidazole solvation shells in the MS-EVB state-selection algorithm.

Given the delocalized nature of the excess proton charge defect, its position can be defined as the center of excess charge (CEC). This vector is expressed as

$$\boldsymbol{r}_{CEC} = \sum_{i}^{N} c_i^2 \boldsymbol{r}_{COC}^i \tag{14}$$

where c_i^2 is the amplitude of EVB state i and $\boldsymbol{r}_{COC}^i$ is its center of charge. The excess proton self-diffusion coefficient can be calculated from the mean-square displacement (MSD) of the CEC according to the Einstein relation valid at long time

$$D_{CEC} = \frac{\langle |\boldsymbol{r}_{CEC}(t) - \boldsymbol{r}_{CEC}(0)|^2 \rangle}{6t} \tag{15}$$

Figure 9 shows the MSD of the CEC at 393 K as a function of time. The self-diffusion coefficient D_{CEC} is calculated to be 0.20 ± 0.01 Å²/ps, in good agreement with the experimental value of 0.20 Å²/ps.[10] To quantitatively examine the effect of proton charge defect delocalization on proton mobility, we also calculated the diffusion coefficient of classical imidazolium with the Grotthuss shuttling mechanism disabled in the MS-EVB algorithm. At 393 K, its value is calculated to be 0.14 ± 0.01 Å²/ps (Figure 9). Grotthuss shuttling therefore enhances proton diffusion by ~40%; therefore, the effects of proton charge defect delocalization and hopping in liquid imidazole are certainly not negligible despite the dominant population of fully localized imidazolium.

The activation energy E_{act}, usually considered the energy barrier for a chemical reaction, can be calculated by linearly

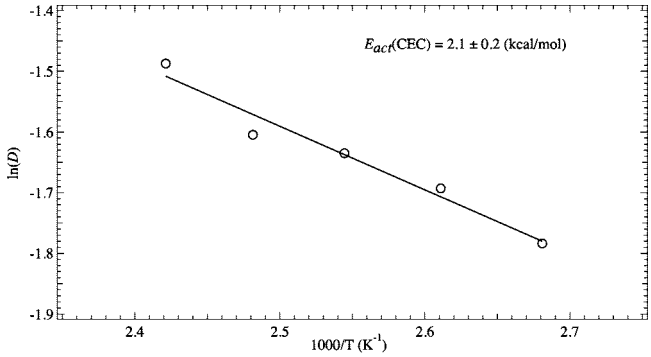

Figure 10. Inverse temperature dependence of the proton self-diffusion coefficient.

fitting ln(D) as a function of 1/T. In the present E_{act} calculation, additional simulations were performed at 373, 383, 403, and 413 K. The value of E_{act} obtained from these data (Figure 10) turns out to be 2.1 kcal/mol, substantially smaller than the activation energy of 5.3 kcal/mol for proton diffusion in pure liquid imidazole without an excess proton.[2] The lower activation energy for the excess proton diffusion can be ascribed to a change in which the step limits the proton-transfer rate; imidazole molecules alone must rely on energetically costly self-ionization,[61] while the presence of an excess proton permits the relatively inexpensive reorientation of imidazole rings.[24]

3.7. Proton-Hopping Rate. Because proton "hopping" transport in protonated imidazole can be regarded as an evolution of the imidazolium identity over time, its rate can be characterized using the successful proton-hopping events. Two distinct types of proton hopping were observed in the MS-EVB simulations. The first type, oscillatory shuttling, occurs when the excess proton hops back and forth between the imidazolium molecule and its first solvation shell imidazoles. The second type, arising from Grotthuss shuttling, occurs when the excess proton hops from an imidazolium formed from a first solvation shell imidazole to a second solvation shell imidazole. As Grotthuss shuttling will contribute the most to the proton-hopping transport mechanism, it will be extensively investigated.

Grotthuss-type hopping, also called forward hopping, can be monitored by a stepwise accumulation function

$$\begin{cases} h(t) = h(t-1) + \Delta h(\Delta t) \\ h(0) = 0 \end{cases} \tag{16}$$

where Δt is the time step. The increment function $\Delta h(\Delta t)$ is defined as

$$\Delta h(\Delta t) = \begin{cases} 0 & \text{if no proton hopping} \\ 1 & \text{if proton hops to a new imidazole} \\ -1 & \text{if proton hops to the prior imidazole} \end{cases} \tag{17}$$

Note that in the third case of eq 17, when the proton returns to the prior imidazole, the imidazole from which it just hopped becomes the new prior imidazole for the next time step.

By examining the profile of the accumulation function $h(t)$, the two types of proton hopping can be distinguished. A profile of $h(t)$ for a randomly selected MS-EVB trajectory at 393 K is shown in Figure 11. Although oscillatory proton shuttling is much less frequent in imidazole than that in water, it still occurs quite often, particularly during "long resting" periods when little to no forward proton hopping takes place. Typical long resting

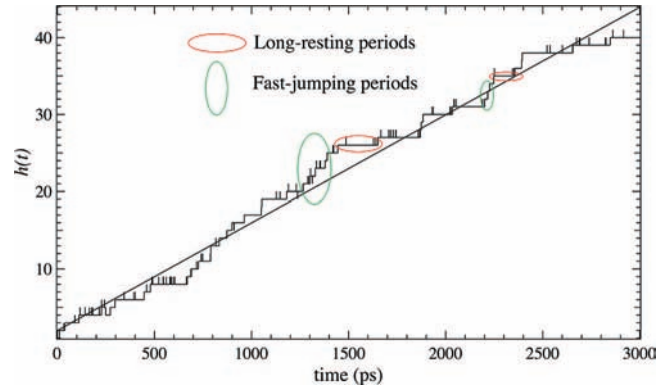

Figure 11. The proton forward-hopping function, eq 16, of a randomly selected MS-EVB constant NVE trajectory with a target temperature of 393 K.

periods are indicated by red ellipses in Figure 11. It is interesting to note that a "fast jumping" period of 100−1000 ps duration is usually present between two long resting periods. During fast jumping periods (green ellipses), a substantial number of forward hops were observed but with little oscillatory shuttling, as demonstrated in Figure 11. This pattern suggests that it may take a relatively long time for the imidazole molecules to orient themselves in a way that favorably accommodates the formation of a new imidazolium cation through fast Grotthuss shuttling. In this latter case, it would be imidazole ring orientation rather than hydrogen bond oscillation that ultimately limits the forward-hopping rate, on which the proton self-diffusion coefficient is significantly dependent. A linear fit to $h(t)$ reveals that the forward-hopping rate was ∼1/72 ps^{-1}. Given that the two nitrogen atoms of the pivot imidazolium are chemically equivalent, the backward-hopping rate is obviously the same. The overall hopping rate is thus twice as much as the forward-hopping rate, or 1/36 ps^{-1} at 393 K. This result is in reasonable agreement with the experimentally estimated value of 1/30 ps^{-1}.[10]

The time scale of the imidazole ring reorientation in the liquid phase can be determined from the autocorrelation function of its normal vector, $C(t)$, which is given by

$$C(t) = \sum_{i=1}^{N} \langle \cos(\theta_i(t)) \rangle \tag{18}$$

where N is the total number of imidazole rings in the system and $\theta_i(t)$ is the rotation angle of the normal vector of the ith imidazole ring at time t. In the present study, the normal vector of an imidazole ring was defined as the cross product of vector $\vec{v}_{N1-C2}$, which connects atom N1 and atom C2, and vector, $\vec{v}_{N2-C2}$, which connects atom N2 and atom C2. At 393K, $C(t)$ decays to 0 in ∼20 ps, which can be regarded as the time scale of the imidazole ring reorientation. The agreement in time scale between the Grotthuss-type proton hopping and the imidazole ring reorientation suggests that the formation of new hydrogen bonds through ring reorientation determines the transport rate for an excess proton in liquid imidazole.

4. Concluding Remarks

The amphoteric imidazole molecule, which can either donate or accept an excess proton, has the potential to serve as a component of anhydrous polyelectrolyte membranes used in new fuel cell designs.[62] Infrared spectroscopy of liquid imidazole

has revealed an extensive hydrogen-bonding network,[61] implying that excess protons can be relayed between imidazole molecules through ring reorientation.[1] If true, charge defect delocalization and Grotthuss shuttling may be as essential to proton transfer in liquid imidazole as they are in the more widely investigated aqueous solutions.

The present study has developed a reactive molecular force field within the MS-EVB framework to describe proton transport in protonated liquid imidazole. Although the MS-EVB model was calibrated in part using the ab initio PES of a gas-phase protonated imidazole dimer, it provides liquid-phase properties (proton diffusion coefficient and Grotthuss hopping rate) in good agreement with experimental results. Importantly, the second imidazole solvation shell of the pivot imidazolium is shown to be substantially disordered. This result suggests that proton hopping in this system is a highly localized process, involving only those few imidazole molecules closest to the imidazolium cation having the excess proton.

It is suggested here that the proton-transfer rate is principally dependent on how rapidly the highly ordered first imidazole solvation shell can be formed around a newly established imidazolium cation. Such a dynamic solvation structure highlights the importance of the process of ring reorientation following a Grotthuss-type proton hop. Also, on the basis of this efficient proton-transport mechanism observed in protonated liquid imidazole, it is not surprising that much more efficient proton conduction has also been observed in polymer electrolytes by mixing the amphoteric heterocyclic compounds with a small amount of protonic acid, for example, H_2SO_4.[10] The acid likely lowers the viscosity of the system in addition to increasing the protonic defect concentration. In this spirit, admixtures of imidazole and room-temperature ionic liquids are also a promising means of enhancing proton mobility and thermostability.[12] Encouraging results have demonstrated that a combination of ionic liquids and imidazole derivatives can achieve proton conductivity as high as that found in aqueous solutions.[63] These interesting systems will be investigated using the imidazole MS-EVB model developed here in the future.

Acknowledgment. This research was supported by the Department of Energy Office of Basic Energy Sciences (Grant No. DE-FG02-05ER15724) for G.A.V. and by the National Natural Science Foundation of China (Grant No. 20503013) for T.Y. The computational resources utilized in this research by G.A.V. were supported under the following NSF programs: Partnerships for Advanced Computational Infrastructure, the Distributed Terascale Facility (DTF), and Terascale Extensions: Enhancement to the Extensible Terascale Facility.

References and Notes

(1) Daycock, J. T.; Jones, G. P.; Evans, J. R. N.; Thomas, J. M. *Nature* **1968**, *218*, 672.
(2) Kawada, A.; McGhie, A. R.; Labes, M. M. *J. Chem. Phys.* **1970**, *52*, 3121.
(3) Brédas, J. L.; Poskin, M. P.; Delhalle, J.; André, J. M.; Chojnacki, H. *J. Phys. Chem.* **1984**, *88*, 5882.
(4) Maupin, C. M.; Wong, K. F.; Soudackov, A. V.; Kim, S.; Voth, G. A. *J. Phys. Chem. A* **2006**, *110*, 631.
(5) Kreuer, K. D.; Paddison, S. J.; Spohr, E.; Schuster, M. *Chem. Rev.* **2004**, *104*, 4637.
(6) Rozière, J.; Jones, D. J. *Annu. Rev. Mater. Res.* **2003**, *33*, 503.
(7) Kreuer, K. D. *ChemPhysChem* **2002**, *3*, 771.
(8) Steininger, H.; Schuster, M.; Kreuer, K. D.; Kaltbeitzel, B. B.; Bingöl, B.; Meyer, W. H.; Schauff, S.; Brunklaus, G.; Maier, J.; Spiess, H. W. *Phys. Chem. Chem. Phys.* **2007**, *9*, 1764.
(9) Ralph, E. K., III; Grunwald, E. *J. Am. Chem. Soc.* **1968**, *90*, 517.
(10) Kreuer, K. D.; Fuchs, A.; Ise, M.; Spaeth, M.; Maier, J. *Electrochim. Acta* **1998**, *43*, 1281.
(11) Sun, J.; Jordan, L. R.; Forsyth, M.; MacFarlane, D. R. *Electrochim. Acta* **2001**, *46*, 1703.
(12) Noda, A.; Susan, M. A. B. H.; Kudo, K.; Mitsushima, S.; Hayamizu, K.; Watanabe, M. *J. Phys. Chem. B* **2003**, *107*, 4024.
(13) Ogihara, W.; Kosukegawa, H.; Ohno, H. *Chem. Commun.* **2006**, *34*, 3637.
(14) Sekhon, S. S.; Lalia, B. S.; Park, J.-S.; Kim, C.-S.; Yamada, K. *J. Mater. Chem.* **2006**, *16*, 2256.
(15) Sekhon, S. S.; Krishnan, P.; Singh, B.; Yamada, K.; Kim, C.-S. *Electrochim. Acta* **2006**, *52*, 1639.
(16) Ohno, H.; Yoshizawa, M.; Ogihara, W. *Electrochim. Acta* **2004**, *50*, 255.
(17) Schuster, M.; Meyer, W. H.; Wegner, G.; Herz, H. G.; Ise, M.; Schuster, M.; Kreuer, K. D.; Maier, J. *Solid State Ionics* **2001**, *145*, 85.
(18) Schuster, M. F. H.; Meyer, W. H.; Schuster, M.; Kreuer, K. D. *Chem. Mater.* **2004**, *16*, 329.
(19) Li, S.; Zhou, Z.; Zhang, Y.; Liu, M. *Chem. Mater.* **2005**, *17*, 5884.
(20) Zhou, Z.; Li, S.; Zhang, Y.; Liu, M.; Li, W. *J. Am. Chem. Soc.* **2005**, *127*, 10824.
(21) Zhou, Z.; Liu, R.; Wang, J.; Li, S.; Liu, M.; Brédas, J.-L. *J. Phys. Chem. A* **2006**, *110*, 2322.
(22) de Grotthuss, C. J. T. *Ann. Chim.* **1806**, *LVIII*, 54.
(23) Agmon, N. *Chem. Phys. Lett.* **1995**, *244*, 456.
(24) Münch, W.; Kreuer, K. D.; Silvestri, W.; Maier, J.; Seifert, G. *Solid State Ionics* **2001**, *145*, 437.
(25) Susan, M. A. B. H.; Noda, A.; Mitsushima, S.; Watanabe, M. *Chem. Commun.* **2003**, 938.
(26) Hickman, B. S.; Mascal, M.; Titman, J. J.; Wood, I. G. *J. Am. Chem. Soc.* **1999**, *121*, 11486.
(27) Goward, G. R.; Schuster, M. F. H.; Sebastiani, D.; Schnell, I.; Spiess, H. W. *J. Phys. Chem. B* **2002**, *106*, 9322.
(28) Fischbach, I.; Spiess, H. W.; Saalwächter, K.; Goward, G. R. *J. Phys. Chem. B* **2004**, *108*, 18500.
(29) Goward, G. R.; Saalwächter, K.; Fischbach, I.; Spiess, H. W. *Solid State NMR* **2003**, *24*, 150.
(30) Benhabbour, S. R.; Chapman, R. P.; Scharfenberger, G.; Meyer, W. H.; Goward, G. R. *Chem. Mater.* **2005**, *17*, 1605.
(31) Iannuzzi, M.; Parrinello, M. *Phys. Rev. Lett.* **2004**, *93*, 025901.
(32) Iannuzzi, M. *J. Chem. Phys.* **2006**, *124*, 204710.
(33) Scheiner, S.; Yi, M. *J. Phys. Chem.* **1996**, *100*, 9235.
(34) Yan, S.; Bu, Y.; Cao, Z.; Li, P. *J. Phys. Chem. A* **2004**, *108*, 7038.
(35) Deng, W.-Q.; Molinero, V.; Goddard III, W. A. *J. Am. Chem. Soc.* **2004**, *126*, 15644.
(36) Paddison, S. J.; Kreuer, K. D.; Maier, J. *Phys. Chem. Chem. Phys.* **2006**, *8*, 4530.
(37) Voth, G. A. *Acc. Chem. Res.* **2006**, *39*, 143.
(38) Swanson, J. M. J.; Maupin, C. M.; Chen, H.; Petersen, M. K.; Xu, J.; Wu, Y.; Voth, G. A. *J. Phys. Chem. B* **2007**, *111*, 4300.
(39) Tuckerman, M.; Laasonen, K.; Sprik, M.; Parrinello, M. *J. Chem. Phys.* **1995**, *103*, 150.
(40) Marx, D. *ChemPhysChem.* **2006**, *7*, 1848.
(41) Laio, A.; Parrinello, M. *Proc. Natl. Acad. Sci. U.S.A.* **2002**, *99*, 12562.
(42) Schuster, M.; Rager, T.; Noda, A.; Kreuer, K. D.; Maier, J. *Fuel Cells* **2005**, *5*, 355.
(43) Lill, M. A.; Helms, V. *J. Chem. Phys.* **2001**, *115*, 7985.
(44) Schmitt, U. W.; Voth, G. A. *J. Chem. Phys.* **1999**, *111*, 9361.
(45) Day, T. J. F.; Soudackov, A. V.; Čuma, M.; Schmitt, U. W.; Voth, G. A. *J. Chem. Phys.* **2002**, *117*, 5839.
(46) Wu, Y.; Chen, H.; Wang, F.; Paesani, F.; Voth, G. A. *J. Phys. Chem. B* **2008**, *112*, 467.
(47) Wang, J.; Wolf, R. M.; Caldwell, J. W.; Kollman, P. A.; Case, D. A. *J. Comput. Chem.* **2004**, *25*, 1157.
(48) Wang, J.; Wang, W.; Kollman, P. A.; Case, D. A. *J. Mol. Graph. Model.* **2006**, *25*, 247.
(49) Alagona, G.; Ghio, C.; Monti, S. *Phys. Chem. Chem. Phys.* **2004**, *6*, 2849.
(50) Mayo, S. L.; Olafson, B. D.; Goddard, W. A. *J. Phys. Chem.* **1990**, *94*, 8897.
(51) Bayly, C. I.; Cieplak, P.; Cornell, W. D.; Kollman, P. A. *J. Phys. Chem.* **1993**, *97*, 10269.
(52) Cornell, W. D.; Cieplak, P.; Bayly, C. I.; Kollman, P. A. *J. Am. Chem. Soc.* **1993**, *115*, 9620.
(53) Katritzky, A. R.; Ghiviriga, I.; Oniciu, D. C.; O'Ferrall, R. A. M.; Walsh, S. M. *J. Chem. Soc. Perkin Trans. 2* **1997**, 2605.
(54) Frisch, M. J.; Trucks, G. W.; Schlegel, H. B.; Scuseria, G. E.; Robb, M. A.; Cheeseman, J. R.; Montgomery, J. A., Jr.; Vreven, T.; Kudin, K. N.; Burant, J. C.; Millam, J. M.; Iyengar, S. S.; Tomasi, J.; Barone, V.; Mennucci, B.; Cossi, M.; Scalmani, G.; Rega, N.; Petersson, G. A.; Nakatsuji, H.; Hada, M.; Ehara, M.; Toyota, K.; Fukuda, R.; Hasegawa, J.; Ishida, M.; Nakajima, T.; Honda, Y.; Kitao, O.; Nakai, H.; Klene, M.; Li, X.; Knox, J. E.; Hratchian, H. P.; Cross, J. B.; Adamo, C.; Jaramillo, J.; Gomperts, R.; Stratmann, R. E.; Yazyev, O.; Austin, A. J.; Cammi, R.;

Pomelli, C.; Ochterski, J. W.; Ayala, P. Y.; Morokuma, K.; Voth, G. A.; Salvador, P.; Dannenberg, J. J.; Zakrzewski, V. G.; Dapprich, S.; Daniels, A. D.; Strain, M. C.; Farkas, O.; Malick, D. K.; Rabuck, A. D.; Raghavachari, K.; Foresman, J. B.; Ortiz, J. V.; Cui, Q.; Baboul, A. G.; Clifford, S.; Cioslowski, J.; Stefanov, B. B.; Liu, G.; Liashenko, A.; Piskorz, P.; Komaromi, I.; Martin, R. L.; Fox, D. J.; Keith, T.; Al-Laham, M. A.; Peng, C. Y.; Nanayakkara, A.; Challacombe, M.; Gill, P. M. W.; Johnson, B.; Chen, W.; Wong, M. W.; Gonzalez, C.; Pople, J. A. *Gaussian 03*, revision C.02; Gaussian, Inc.: Wallingford, CT, 2004.

(55) Press, W. H.; Flannery, B. P.; Teukolsky, S. A.; Vetterling, W. T. *Numerical Recipes in FORTRAN 77: The Art of Scientific Computing*, 2nd ed.; Cambridge University Press: Cambridge, U.K., 1992.

(56) Lide, D. R., Ed. Physical Constants of Organic Compounds. In *Handbook of Chemistry and Physics*, 88th ed.; CRC Press: Boca Raton, FL, 2007.

(57) Hoover, W. G. *Phys. Rev. A* **1985**, *31*, 1695.

(58) Allen, M. P.; Tildesley, D. J. *Computer Simulation of Liquids*, 2nd ed.; Oxford University Press: New York, 1989.

(59) Smith, W.; Forester, T. R. *J. Mol. Graphics* **1996**, *14*, 136.

(60) Markovitch, O.; Chen, H.; Izvekov, S.; Paesani, F.; Voth, G. A.; Agmon, N. *J. Phys. Chem. B* **2008**, *112*, 9456.

(61) Perchard, C.; Novak, A. *J. Chem. Phys.* **1968**, *48*, 3079.

(62) Schuster, M. F. H.; Meyer, W. H. *Ann. Rev. Mater. Res.* **2003**, *33*, 233.

(63) Xu, W.; Angell, C. A. *Science* **2003**, *302*, 422.

JP811156R